JOURNAL OF THE AMERICAN CHEMICAL SOCIETY

Article

Inverting Steric Effects: Using 'Attractive' Non-Covalent Interactions to Direct Silver-Catalyzed Nitrene Transfer

Minxue Huang, Tzuhsiung Yang, Jon Paretsky, John F. Berry, and Jennifer M Schomaker

J. Am. Chem. Soc., **Just Accepted Manuscript** • DOI: 10.1021/jacs.7b07619 • Publication Date (Web): 01 Nov 2017

Inverting Steric Effects: Using 'Attractive' Non-Covalent Interactions to Direct Silver-Catalyzed Nitrene Transfer

Minxue Huang‡, Tzuhsiung Yang‡, Jon Paretsky, John F. Berry* and Jennifer M. Schomaker*

Department of Chemistry, University of Wisconsin, Madison, Wisconsin 53706, United States

Supporting Information Placeholder

ABSTRACT: Nitrene transfer (NT) reactions represent powerful and direct methods to convert C–H bonds into amine groups that are prevalent in many commodity chemicals and pharmaceuticals. The importance of the C–N bond has stimulated the development of numerous transition metal complexes to effect chemo-, regio- and diastereoselective NT. An ongoing challenge is to understand how subtle interactions between catalyst and substrate influence the site-selectivity of the C–H amination event. In this work, we explore the underlying reasons why Ag(tpa)OTf (tpa = tris(pyridylmethyl)amine) prefers to activate α-conjugated C–H bonds over 3° alkyl C(sp^3)–H bonds and apply these insights to reaction optimization and catalyst design. Experimental results suggest possible roles of non-covalent interactions (NCIs) in directing the NT; computational studies support the involvement of π···π and Ag···π interactions between catalyst and substrate, primarily by lowering the energy of the directed transition state and reaction conformers. A simple Hess's law relationship can be employed to predict selectivities for new substrates containing competing NCIs. The insights presented herein are poised to inspire the design of other catalyst-controlled C–H functionalization reactions.

Introduction.

Strategies for the selective functionalization of C–H bonds can be grouped into two broad categories, consisting of directed and non-directed reactions. The former approach relies on the association of a substrate to a metal center, typically through a polar functional group, to facilitate the activation of a specific proximal C–H bond (Figure 1A).[1] In contrast, non-directed strategies generate transient and highly reactive metal-containing intermediates; these engage with C–H bonds largely based on inherent steric and electronic preferences dictated by the substrate.[2] Group transfer reactions, including metal-catalyzed nitrene transfer reactions (NT), have traditionally fallen into the latter category (Figure 1B).

Transition metal-catalyzed NT represents a convenient method for directly transforming C–H bonds to valuable C–N bonds.[3,4-11] Recent progress in C–H amination via NT has focused mainly on situations where individual C–H bonds display reasonable differences in terms of their intrinsic electronic, steric or stereoelectronic features.[12] In these scenarios, *repulsive* non-covalent interactions (NCIs) between the catalyst and substrate are used to alter the selectivity of the reaction (Figure 1C).[13] A complementary, but underexplored, approach is to build *attractive* NCIs into a substrate/catalyst combination (Figure 1D).[14] As an example, hydrogen-bonding between a porphyrin-supported Co catalyst and a nitrene generated from $PhSO_2N_3$ has been demonstrated by Zhang and de Bruin to accelerate the rate of olefin aziridination.[15] In effect, this strategy enables the NT event to be 'directed' via a NCI; however, to our knowledge, the fundamental question of whether the inherent selectivity of C–H functionalization proceeding through NT can be enhanced or overridden through attractive, non-covalent interactions has not been explicitly addressed.

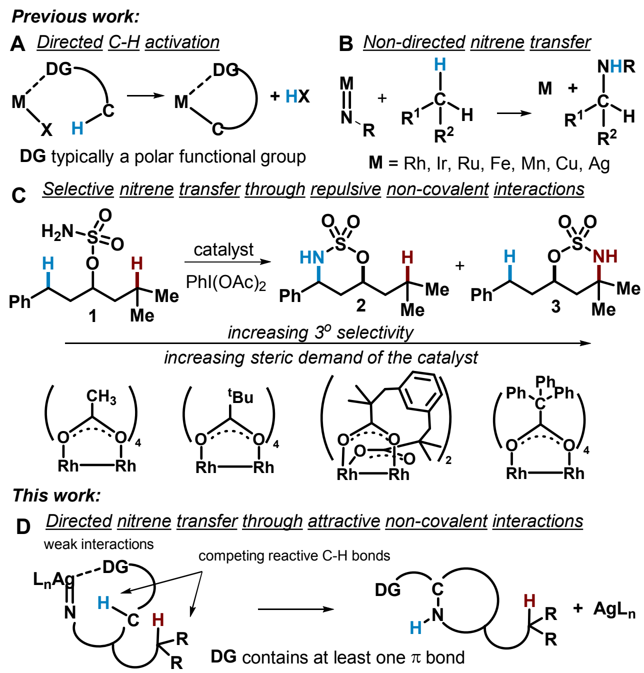

Figure 1. General strategies for C-H functionalization.

Of the transition metals that catalyze NT,[4-11] we selected Ag(I) complexes to study directed amination, due to their diverse coordination environments,[16,17] Lewis acidity and ability to engage in cation-π interactions. Substrates adorned with traditional directing groups, such as pyridines and imines, proved unsuccessful, as strong interactions between Ag and directing group precluded our ability to tune the site of the C–H amination. This led us to consider whether weak attractive NCIs between catalyst and substrate might constitute a more viable design principle to achieve flexible and tunable directed C–H amination. Herein, we report experimental and computational studies supporting the ability of NCIs, including Ag···π and aromatic-aromatic interactions, to influence the outcome of NT reactions.

Computational modeling of NCIs is particularly challenging for current quantum chemical methods.[18] The need to sample multiple conformations and configurations of the reactants and transition states is not straightforward, although for simple systems, this can be dealt with using molecular dynamics simulations.[19] However, for the large Ag complexes studied herein, the use of molecular dynamics is not possible. We have therefore adopted a statistical mechanics approach, where the weighted populations of the key conformations of the catalyst are taken into account and used to calculate product distributions. The insights drawn from these computational studies were implemented in the design of second-generation Ag catalysts with improved preference for the amination of electron-poor benzylic C–H and other α-conjugated C–H bonds, paving the way for new catalysts that effectively harness NCIs to drive selectivity in metal-catalyzed group transfers.

Results and discussion.

We recently reported that Ag(tpa)OTf, a silver complex supported by a tris(2-pyridylmethyl)amine (tpa) ligand, unexpectedly preferred to aminate α-conjugated C–H bonds over 3° alkyl C(sp^3)–H bonds, albeit in moderate selectivities.[17a] Further optimization yielded several observations relevant to a deeper understanding of the mechanism of intramolecular NT promoted by Ag(tpa)OTf, including the possibility that π···π or Ag···π interactions play important roles in directing selectivity.

Mechanistic aspects. The first indication that Ag(tpa)OTf might induce site-selective NT through directing NCIs arose from studies comparing its reactivity with other known NT catalysts. Reactions of **1** (Scheme 1A) with Rh(II)$_2$L$_n$ displayed higher selectivities for **3** as the bridging equatorial ligands on the Rh increased in size.[13] This trend of catalyst-controlled selectivity falls within the paradigm of steric-driven regioselectivity, where the α-phenyl ring of **1** displays greater steric repulsion with the equatorial ligands than the two geminal α-methyl groups (cone angle of 145° for PPh$_3$ *vs.* 118° for P(CH$_3$)$_3$ during the abstraction of the γ C–H bond). On the other hand, Ru and Fe catalysts furnished **2** with varying degrees of selectivity.[8c,20] These results fit the prevailing NT mechanistic paradigm, where catalysts proceeding via stepwise H-transfer/radical recombination (S-HT/RR) tend to show higher kinetic isotope effect (KIE) values (Scheme 1B) and favor amination of weaker C–H bonds (BDE: 2° benzylic C–H ~ 85 kcal/mol; 3° alkyl C(sp^3)–H ~ 95 kcal/mol). However, the range of site-selectivities described in Scheme 1A is curious, suggesting that invoking 'stepwise vs. concerted' mechanisms to explain the observed results does not sufficiently capture subtle interactions that might shape the outcome of the C–H amination.

Ag(tpa)OTf proved an intriguing catalyst for NT; typical mechanistic probes, including KIE and radical clock studies (Scheme 1B), initially appeared to indicate a concerted pathway, similar to Rh(II)$_2$L$_n$ catalysis.[13] However, computational studies carried out by Berry and Musaev showed that a requirement for concerted nitrene transfer is the presence of an empty N-centered orbital on the metal-nitrene intermediate.[21] The triplet ground states of Ag-nitrene intermediates do not permit this condition to be met; thus, reactions catalyzed by Ag(tpa)OTf are electronically prohibited from occurring via concerted pathways. Further computational modeling resolved this discrepancy by showing that Ag-catalyzed NT can proceed via a mechanism we have termed 'elementary hydrogen transfer/radical recombination' (E-HT/RR). This mechanism occurs with a single HT transition state, followed by a radical recombination step displaying no energy barrier; radical species are not stationary points on the potential energy surface.[17e]

In addition to comparisons of the KIE and site-selectivity of metal catalysts for NT (Scheme 1), Hammett studies were carried out with Ag(tpa)OTf (Figure S-1, Supporting Information), giving

Scheme 1. Comparison of metal-catalyzed nitrene transfers.

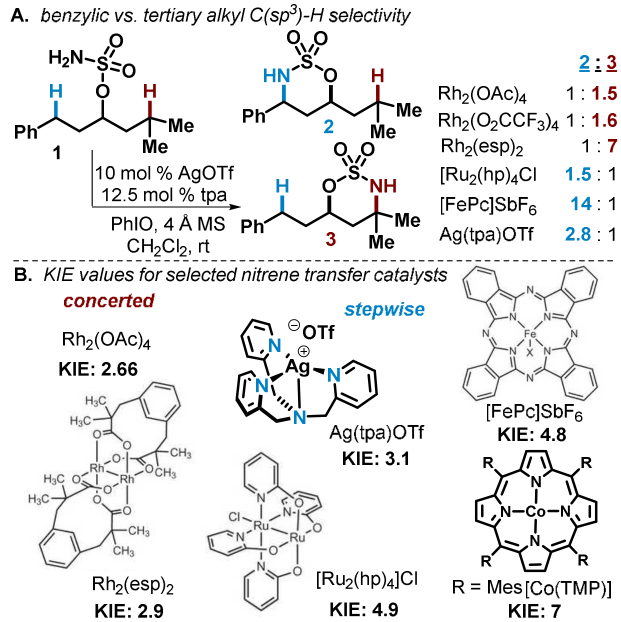

ρ = -0.687 ± 0.024 using σ+ parameters.[22] As with all metal-catalyzed NT reactions reported to date, the negative ρ value indicates a build-up of positive charge in the transition state (TS).[13,17a,20] These results imply an earlier TS for reactions catalyzed by Ag(tpa)OTf, as compared to other catalysts proceeding via stepwise NT; however, the exact reasons for these mechanistic differences are currently unclear.[17e]

Interestingly, examination of KIE and Hammett ρ values showed similarities between Ag(tpa)OTf and Rh$_2$L$_n$ (Scheme 1B),[13,17a] yet the selectivity of the former was more reminiscent of the results noted with Ru, Fe and Co complexes.[8c,20,23] While this might be attributed to stepwise NT promoted by Fe, Ru, Co and Ag, we considered the possibility that additional factors might be responsible for the behavior observed with Ag(tpa)OTf. For example, previous studies found that Ag(I) complexes supported by N-donor ligands show highly fluxional behavior in solution, depending on the counteranion and ligand identity.[17g] This dynamic behavior was particularly evident in Ag(tpa)OTf, which may enable it to engage in π···π and Ag···π interactions.

Attractive NCIs between aromatic rings have long been known to play important structural roles in molecular recognition, template-directed synthesis, protein folding and many other key biological processes.[24] The prototypical benzene dimer π···π stacking interaction is on the order of 2-3 kcal/mol, with the two most stable conformations preferring T-shaped or parallel-displaced orientations.[25] In particular, a parallel-displaced orientation between an aryl group of a NT substrate and a pyridyl ring of Ag(tpa)OTf could yield donor-acceptor interactions that effectively stabilize a transition state leading to benzylic C–H amination.[26] In the context of Ag···π interactions, the aryl group of **1** (Scheme 1A) could engage with silver to direct the outcome of the NT event. Indeed, there are numerous examples of complexes containing Ag···π interactions in the solid state; however, to our knowledge, such interactions have not been invoked to control selectivity in Ag-catalyzed group transfer reactions.[14g-h,27]

Experimental probes of non-covalent interactions. NCIs are often sensitive to reaction conditions; thus, studies to assess the impact of the Ag counteranion, solvent, temperature and concentration on the amination of **1** were carried out (Table S-1 in the SI). The effect of the counteranion on selectivity was minimal, suggesting it is not bound to Ag during the key bond-forming event.[17e,i,21] Counteranion-free Ag-nitrene species were also supported by computational studies (*vide infra*).[17e,i] Concentration had little effect on selectivity, while decreasing the temperature from 25 °C to -20 °C improved the **2:3** ratio. A range of aprotic solvents were examined with **1** (Table 1) at 25 °C; the selectivity for **2**:**3** correlated with solvent polarity (Table S-2 in the SI). Overall yields of **2** and **3** were excellent in most cases, as was the *dr* of **2** (>19:1 in all cases). Preference for benzylic amination tracked best with Reichardt E^N_T values, as opposed to other measures of solvent polarity, including dipole moment and dielectric constant.[25,28] E^N_T values are derived by measuring the long-wave UV-vis absorption band of a negative solvachromatic pyridinium-N-phenoxide betaine dye in the solvent of interest.[29]

Table 1. Relationship between **2**:**3** and Reichardt E^N_T values.

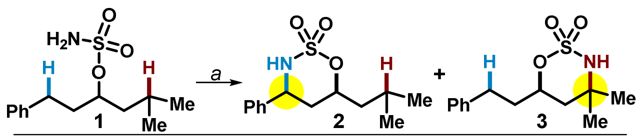

entry	solvent	E^N_T	2 : 3[b]	yield (2+3+Im)[c]
1	CCl_4	0.052	**5.8 : 1**	86%
2	*p*-xylene	0.074	**5.1 : 1**	95%
3	toluene	0.099	**4.8 : 1**	92%
4	benzene	0.111	**4.5 : 1**	>99%
5	Et_2O[d]	0.117	**3.8 : 1**	51% (~49% **1**)
6	PhCl	0.188	**4.2 : 1**	89%
7	EtOAc	0.228	**3.1 : 1**	94%
8	$PhCF_3$[d]	0.241	**3.8 : 1**	91%
9	$CHCl_3$	0.259	**3.5 : 1**	90%
10	CH_2Cl_2	0.309	**2.8 : 1**	91%
11	$(CH_2)_2Cl_2$	0.327	**2.5 : 1**	91%
12	MeCN	0.460	**2.2 : 1**	79%

[a] 10 mol% Ag(tpa)OTf, 3.5 equiv PhIO, 4 Å MS, solvent, 0.05 M, rt, 2 h. [b] Average of 2 trials, imine formed is considered in the ratios. [c] **Im** is the imine formed from overoxidation of **2**. [d] Average of 3 trials.

As previously mentioned, the NCIs most likely to influence the preference for benzylic C–H amination with Ag(tpa)OTf are: 1) π···π interactions between one of the pyridine ligand arms and the aryl group of **1** or 2) Ag···π interactions between Ag and **1**. In the former case, the strength of the π···π interactions is largely influenced by electrostatic attractions between the two aromatic rings or by solvation/desolvation (solvophobic) effects.[28,30] In the aprotic and non-polar solvents employed for our chemistry, electrostatic interactions should dominate, with the strength of the π···π interaction increasing as solvent polarity decreases.[28,30,31] This is observed experimentally in moving from less polar solvents, such as CCl_4 (Table 1, entry 1), to solvents of increasing E^N_T such as benzene, $PhCF_3$ and $CHCl_3$ (entries 4, 8-9). However, if Ag···π interactions are invoked as the primary NCI controlling preference for benzylic C–H amination, sufficient space around the Ag must be available to accommodate engagement of the substrate with the metal. Based on our knowledge of solution-state structures of Ag(tpa)OTf, this is unlikely when the π donor is a large aryl group; however, such interactions may play a significant role in substrates with less sterically demanding π donors, such as alkenes and alkynes (*vide infra*).[17g]

Experimental evidence suggesting NCIs play roles in selective NT into benzylic C–H bonds. Given that solvent effects influence the effectiveness of NCIs, we were curious if the preference for reaction at the benzylic C–H bond of **7-10** could be improved, compared to previous results in CH_2Cl_2 (parentheses in Table 2).[17a] While 1:1 $CHCl_3$:$PhCF_3$ gave the highest selectivity for **2** at -20 °C (Table S-1, entry 9), $CHCl_3$ was adopted for further study. Preference for benzylic C–H amination increased with our new conditions when sterics of the 3° alkyl C(sp^3)–H bond were not overly demanding. Sulfamates **1** and **7-9** showed improved selectivity for **2** and **7a-9a**, respectively, in >19:1 *dr* favoring the *syn* product. Large alkyl substituents, such as the diisopropyl group of **10**, gave only benzylic amination, indicating a steric component largely independent of solvent. While selectivity gains are modest, they do represent >10% increases in yield, render purification of product mixtures easier and support the possibility of π···π interactions between the tpa ligand and the substrate aryl group.

Table 2. Selectivity for NT in competing 2° benzylic vs. 3° alkyl C(sp^3)–H bond aminations with Ag(tpa)OTf.

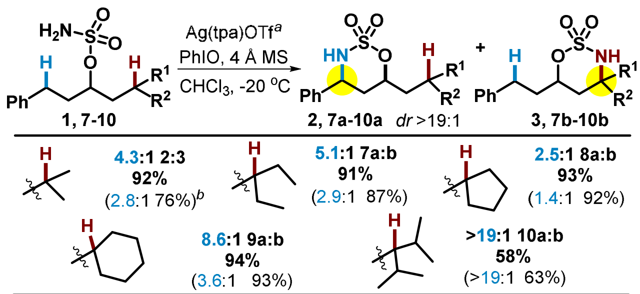

[a] 10 mol% Ag(tpa)OTf formed by combining 10 mol % AgOTf and 12.5 mol % tpa. [b] Previous results in CH_2Cl_2 at rt are shown in parenthesis.

The lower C–H BDEs of benzylic C–H (~82-83 kcal/mol) vs. 3° alkyl C(sp^3)–H bonds (~95 kcal/mol) could also explain the improved selectivities in Table 2. As Ag-catalyzed NT is stepwise in nature, preferential reaction at the weaker C–H bond might be expected.[17e] However, evidence that BDE is not the primary determinant of site-selectivity is shown by minimal changes to **2:3** as the electronics of the tpa ligand are modified (Scheme 2, entries 1-4). In contrast, preference for **3** using Ag(*o*-Me)$_3$tpa(OTf) (entry 5) is due to changes in the preferred conformation of the active catalyst, likely preventing the presence of NCIs between the substrate and catalyst.[17g]

Scheme 2. Ligand identity influences site-selectivity.

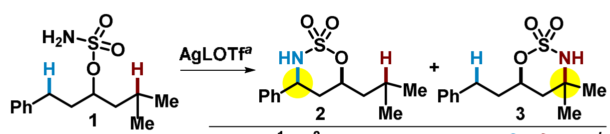

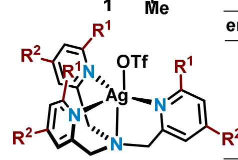

entry	R¹	R²	catalyst	2 : 3	yield[b]
1	H	H	Ag(tpa)OTf	**2.8** : 1	76%
2	H	Cl	Ag(*p*-Cl)$_3$tpa(OTf)	**2.5** : 1	91%
3	H	OMe	Ag(*p*-OMe)$_3$tpa(OTf)	**2.5** : 1	85%
4	H	NMe_2	Ag(*p*-NMe_2)$_3$tpa(OTf)	**2.5** : 1	89%
5	Me	H	Ag(*o*-Me)$_3$tpa(OTf)	1 : **2.1**	72%

[a] 10 mol % catalyst, 3.5 equiv PhIO, 4 Å MS, 0.05 M CH_2Cl_2. [b] Isolated yields.

Testing the possibility of directing π···π interactions in NT reactions through modified tpa ligands. To test if π···π interactions drive a preference for benzylic C–H amination, ligand/substrate combinations were designed to amplify these proposed NCIs. Tpa ligands with electron-donating or withdrawing groups were prepared, as exemplified by (*p*-Me_2N)$_3$tpa, (*p*-MeO)$_3$tpa, and (*p*-Cl)$_3$tpa (SI for details). The performance of Ag(tpa)OTf was benchmarked in entries 1-3 (Table 3), showing that the **2**:**3** ratio increased from 2.8:1 to 4.3:1 in moving from CH_2Cl_2 to $CHCl_3$ at -20 °C. Data for $CHCl_3$ could not be collected at rt, due to formation of the N-chloramine of **2**. Interestingly, an increase in selectivity was not noted with Ag(*p*-$Me_2N)_3$tpa(OTf) (entries 4-6); in fact, the reaction rate decreased in $CHCl_3$ (entry 6). Based on our previous studies of the dynamic behavior of Ag(I) complexes in solution,[17g] we propose that a shift in dynamic equilibrium favors tetradentate binding of (*p*-$Me_2N)_3$tpa to Ag, in contrast to the largely tridentate binding preferred by the parent tpa ligand. The electron-rich nature of (*p*-$Me_2N)_3$tpa, coupled with the decreased fluxionality of Ag(*p*-$Me_2N)_3$tpa(OTf) at -20 °C in $CHCl_3$, results in little change in the **2**:**3** ratio when Ag(tpa)OTf is substituted with Ag(*p*-$Me_2N)_3$tpa(OTf). This fits the argument that π···π interactions play a role in controlling selectivity, as a more electron-rich ligand would not result in increased NCIs with the Ph substituent of **1**. Based on this analysis, Ag(*p*-$Me_2N)_3$tpa(OTf) was not explored with electron-rich **11-12**; rather, changes to the solvent and temperature with Ag(tpa)OTf were adequate to give excellent selectivities for **11a** and **12a** (entries 7-10).

Key results supporting π···π interactions as a viable catalyst design strategy were obtained when substrate and catalyst combinations maximized the impact of NCIs. The presence of electron-poor groups on the aryl moiety of **13** and **14** (entries 11-16) did increase selectivity for **13a** and **14a** with Ag(tpa)OTf (compare entries 11 with 12 and 14 with 15); however, this effect was more pronounced with Ag(*p*-$Me_2N)_3$tpa(OTf) (entries 13, 16). The **13a:b** ratio improved from 3.6:1 using Ag(tpa)OTf to 7.1:1 with Ag(*p*-$Me_2N)_3$tpaOTf in comparable yields and *dr*, favoring the *syn* product (compare entries 12-13). Substrate **14**, with a CF_3 group on the aryl ring, also displayed improved **14a:b** ratios from 1.4:1 with Ag(tpa)OTf to 2.6:1 with Ag(*p*-$Me_2N)_3$tpa(OTf) (compare entries 15-16). Increased benzylic C–H amination of **14** with Ag(*p*-$Me_2N)_3$tpa(OTf) is further corroborated by qualitative reproduction of the experimental results by Density Functional Theory (DFT). Changing the ligand from tpa to (*p*-$Me_2N)_3$tpa resulted in an increase of 1.5 kcal·mol^{-1} in the solvation- and dispersion-corrected electronic driving force ($\Delta\Delta E_{solv,D3}$) for the benzylic *pro*-(*R*) C–H bond using partially relaxed models. The role of NCIs in driving regioselectivity and *dr* is discussed from a theoretical perspective later in the paper.

Table 3. Effect of ligand identity on the selectivity for 2° benzylic C–H vs. 3° alkyl C(sp^3)–H bond amination.

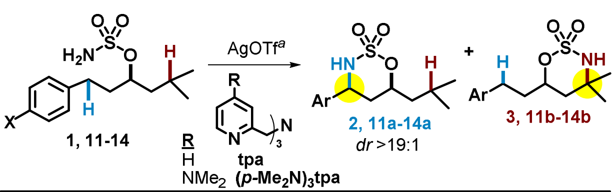

entry	X	ligand	solvent	temp	2:3 or a:b	yield
1	H	tpa	CH_2Cl_2	rt	2.8:1 2:3	76%
2	H	tpa	CH_2Cl_2	-20 °C	3.5:1 2:3	94%
3	H	tpa	$CHCl_3$	-20 °C	4.3:1 2:3	92%
4	H	(*p*-$Me_2N)_3$tpa	CH_2Cl_2	rt	2.5:1 2:3	89%[b]
5	H	(*p*-$Me_2N)_3$tpa	CH_2Cl_2	-20 °C	2.8:1 2:3	87%[b]
6	H	(*p*-$Me_2N)_3$tpa	$CHCl_3$	-20 °C	2.7:1 2:3	37%[b,c]
7	OMe	tpa	CH_2Cl_2	rt	4.7:1 11a:b	85%
8	OMe	tpa	$CHCl_3$	-20 °C	>19:1 11a:b	84%
9	Me	tpa	CH_2Cl_2	rt	4.4:1 12a:b	81%
10	Me	tpa	$CHCl_3$	-20 °C	8.8:1 12a:b	89%
11	Br	tpa	CH_2Cl_2	rt	1.8:1 13a:b	88%
12	Br	tpa	$CHCl_3$	-20 °C	3.6:1 13a:b	84%
13	Br	(*p*-$Me_2N)_3$tpa	CH_2Cl_2	-20 °C	7.1:1 13a:b	83%
14	CF_3	tpa	CH_2Cl_2	rt	1:1.3 14a:b	96%
15	CF_3	tpa	$CHCl_3$	-20 °C	1.4:1 14a:b	92%
16	CF_3	(*p*-$Me_2N)_3$tpa	CH_2Cl_2	-20 °C	2.6:1 14a:b	86%

[a] 10 mol % AgOTf, 12.5 mol % ligand, 3.5 equiv PhIO, 4 Å MS, rt or -20 °C, 2 h. [b] NMR yield, $PhSiMe_3$ internal standard. [c] 51% recovered **1**.

Another explanation for the increased preference for electron-poor benzylic C–H bonds over competing 3° alkyl C(sp^3)–H bonds in **13** and **14** is the stabilization of the putative Ag-nitrene by the electron-rich ($Me_2N)_3$tpa ligand. This would render the Ag nitrene more radical-like and potentially more selective. Increased radical-like character might be reflected in the KIE for the reaction; however, comparing KIEs for Ag(tpa)OTf and Ag(*p*-$Me_2N)_3$tpa(OTf) showed no difference within experimental error.

Experimental evidence suggesting a role for NCIs in the preferred selectivity for NT into allylic and propargylic C–H bonds. We next turned our attention to explaining the preference for amination of allylic and propargylic C-H over 3° alkyl C(sp^3)–H bonds. Ag···π interactions involving acyclic π bonds are well-known;[27] interactions between a silver cation and ethene were first described by Dewar as long ago as 1951.[27a] Similar to π···π interactions, Ag···π interactions are relatively weak, at approximately 1–3 kcal/mol of energetic stabilization.[32]

The possibility of directing Ag···π NCIs via the π-donor capability of alkenes and alkynes was investigated through competitive NT comparing the reactivity of allylic and propargylic C–H bonds *vs.* 3° alkyl C(sp^3)–H bonds (Table 4). In alkenes **11-13**, good chemo- and site-selectivities for allylic C–H amination gave **15a-17a** with high *syn dr*. Similar to Table 2, the lower C–H BDE of allylic C–H (~82-83 kcal/mol) vs. competing 3° alkyl C(sp^3)–H bonds (~95 kcal/mol) may impact reaction outcome. However, we were surprised to find that the preference for amination of propargylic C–H bonds in **18** and **19** was lower than expected, despite decreased sterics and similar BDE (~85 kcal/mol) to allylic and benzylic C–H bonds. These unexpected results were explored through computational studies, as described in the next section.

Table 4. NT selectivity in competing 2° allylic and propargylic C–H vs. 3° alkyl C(sp^3)–H bond aminations with Ag(tpa)OTf.

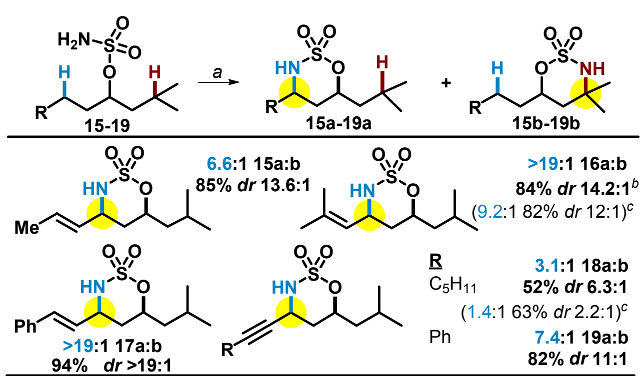

[a] 10 mol % AgOTf, 12.5 mol % tpa, 3.5 equiv PhIO, 0.05 M $CHCl_3$, 4 Å MS, -20 °C. [b] 5% rearranged aziridine. [c] Previous conditions using CH_2Cl_2 at rt.

Computational modeling of multiple catalyst conformations in silver-catalyzed intramolecular nitrene transfer (NT). Exploiting NCIs for catalyst-controlled, site–selective NT is challenging, as these interactions are weak compared to covalent bonds. In addition, multiple conformations with similar energies may be accessible within a targeted catalyst structure. The prediction of major conformations based on conceptually designed catalyst structures are aided by quantum chemical methods, where DFT can examine the presence of NCIs in the context of both catalyst design and the physical understanding of catalysis.[14] One caveat to computational design or rationalization of NCIs in known catalysts is that DFT cannot describe important long-range electron correlation.[18a-c] Such correlation can be recovered by: 1) including a fixed amount of Hartree-Fock exchange (HFX) in the density functional to give global hybrid functionals such as the popular B3LYP, used in this study for geometry optimizations and frequency calculations, or 2) using a variable amount of HFX to give a range-separated hybrid functional such as *w*B97X, used in this study for single point energies.[33] Empirical corrections, such as DFT-D3 used in this study, further improve the recovery of long-range correlation.[18d] We use these methods here to make structural and energetic models of NCIs between catalysts and substrates at the level of DFT.

The weak nature of NCIs means that both non-directed and directed conformations of the catalyst-substrate complex are present and catalytically relevant. In the calculations presented herein, the reactive nitrene intermediate (denoted **RC**) exists in two conformations, one predisposed for benzylic amination and the other for reaction at the 3° C–H bond. Considering the general case of a catalyst with conformations $\mathbf{RC_A}$ and $\mathbf{RC_B}$, there are two limiting cases for how these conformations contribute to the product distributions $\mathbf{P_A}$ and $\mathbf{P_B}$, derived from $\mathbf{RC_A}$ and $\mathbf{RC_B}$, respectively. In one case, the reaction is under kinetic control, while the other situation is best described by a Curtin-Hammett situation. In our computational work, the product ratios are calculated under both scenarios to assess whether selectivity of the NT occurs under kinetic-only or Curtin-Hammett-corrected control (see the SI for further details of these models).

Modeling NCIs from Ag(tpa)OTf-nitrene species to C–H amination transition states. To better understand site-selectivity in competing reaction of benzylic vs. 3° alkyl C(sp^3)–H bonds (Table 1), DFT studies were performed on *pro*-benzylic and *pro*-3° conformers of potential Ag-nitrene intermediates, based on the structure of Ag(OTf)tpa. As counteranion identity has little effect, we focused on *pro*-benzylic counteranion-free $[\text{Ag(nitrene)tpa}]^+$ (**RC-1A**) and $[\text{Ag (nitrene)}(\eta^3\text{-tpa})]^+$ complex (**RC-1B**) with one pyridyl arm detached (nitrene = NSO_3-(*S*)-CH(^{i}Bu)(EtPh)), as VT-^{1}H NMR studies of Ag(tpa)OTf show hemilability of the ligand (Figure 2, Fig S-2 for **1C-D**).[17g,j] **RC-1A** is 12.9 kcal·mol^{-1} more stable than **RC-1B**; consistent with previous work, the triplet is the lowest energy state for both structures, with the Ag-nitrene interaction showing partial σ and π bond character.[17e] Ag-nitrene reactant complexes (**RC**s) are best described as Ag(II)-nitrene$^{\bullet-}$ (nitrene$^{\bullet-}$= nitrene radical anion) structures. For all possible Ag-nitrene structures, critical points along the triplet potential surface (^{3}PES) were scanned, and the transition states (**TS**) for either benzylic (both *R* and *S* products are considered) or 3° C-H amination were located. In total, twelve **RC** and **TS** structures were investigated: the *pro*-benzylic and *pro*-3° **RC**s **1A**-**1D** and *R*-benzylic, *S*-benzylic, and 3° **TS**s **1A**-**1D**. Importantly, we found substrate-aryl···tpa-pyridyl π···π interactions between 3.22 and 3.34 Å in **RC**s/**TS**s for both **1A** and **1B**. No such π···π interaction occur in the *pro*-3° structures (**1C**, Figure S-2).

All reactant complexes (**RC**) perform nitrene insertion through an initial H-atom abstraction TS having a near-linear C···H···N structure (160–177°). Comparing the TS energies required to abstract either a benzylic (**Bn**) or 3° (**T**) C–H bond of the substrate in **1A**-**1B**, we found the computed **Bn**:**T** selectivities to be >20:1 and 6.9:1, respectively. In contrast, **1A** and **1B** gave a computed **Bn**:**T** selectivity of 1:20, which does not match the experimental **Bn**:**T** ratio of 4.3:1.

To investigate potential Ag···π NCIs in alkenes, we computed

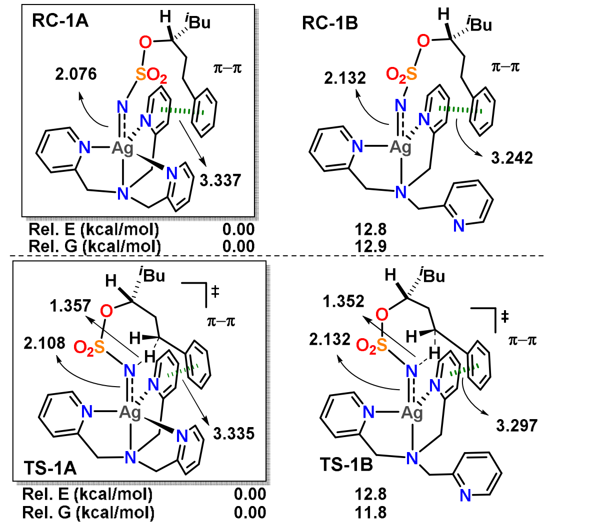

Figure 2. Reactant (top) and benzylic transition state complexes (bottom) of **1A**-**1B** (nitrene = NSO_3-(*S*)-CH(^{i}Bu)(EtPh)). Distances: Å. Relative single point and Gibbs free energies: kcal·mol^{-1}.

the regioselectivity between an allylic C-H and a 3° C-H bond in **2A**-**2D** (Figure 3). These structures are analogous to **1A**-**1D**, where the nitrene = NSO_3-(*S*)-CH(^{i}Bu)(Et-(*E*)-CH=CHMe). As expected, calculations using model **2C** poorly predict selectivity for the 3° over the allylic (**Al**) C-H bond (calc. **T**:**Al** = >20:1, *syn*:*anti* = 1:>20). In contrast, OTf-free *pro*-(*S*) **2A** and **2B** show potential Ag-olefin interactions (Ag···C distances from 3.52-3.60 Å). Calculations on **2A** gave **Al**:**T** = >20:1 and *syn*:*anti* = >20:1, which compare well with experiment, **Al**:**T** = 6.6:1 and *syn*:*anti* = 13.6:1. Preferential activation of the allylic C-H bond in **2A** likely results from an NCI between the Ag cation and the allylic π system. This type of Ag···π interaction is well-documented; in fact, 251 crystal structures of Ag-olefin complexes structures have been reported.[34]

The results for **2B** were at first puzzling, as directing Ag-π interactions were expected to be present based on results observed for **2A**. However, the calculated (**T**:**Al** = >20:1 and *syn*:*anti* = 1:4.8) and experimental (**T**:**Al** = 1:6.6 and *syn:anti* = 13.6:1) results did not agree. The reasons why **2B** prefers activation of the 3° C–H bond will be described later in the discussion.

Interestingly, preferential activation of the 3° C-H bond by **2C** (Figure 3) is reminiscent of $Ag(bpy)_2OTf$, previously reported to prefer 3° C-H over allylic C-H bond amination.[17a] The resemblance between **2C** and $Ag(bpy)_2OTf$ prompted us to investigate the TS of $[\text{Ag(bpy)}_2\text{-nitrene(Al)}]^+$ (**2E**) for comparison. Indeed, **TS-2C** and **TS-2E** display similar structures, where two pyridyl rings lie in the equatorial plane, one pyridyl ring is located in the axial position *trans* to the nitrene and a fourth ligand (a pyridyl ring in **TS-2C** and $^-$OTf anion in **TS-2E**) occupies the third position of a triangle in the equatorial plane. The steric congestion in the equatorial plane points the vinyl group away from the Ag, preventing its interaction with the alkene π electrons. This leads to preferred reaction of the 3° C-H bond over the allylic C-H bond for **2E** (calculated: **T**:**Al** = 5.2:1, *syn*:*anti* = 1.13:1; experiment: **T**:**Al** = 1.1:1, *syn*:*anti* = 3.7:1 (1,1-Me_2allylic C–H bond)).

The unexpected preference for reaction of the 3° C–H bond over the allylic C–H bonds of **2B** is attributed to the η^2-binding mode of the nitrene to the electron-deficient Ag center upon dissociation of a pyridyl arm (Figure 3). This binding mode has been reported

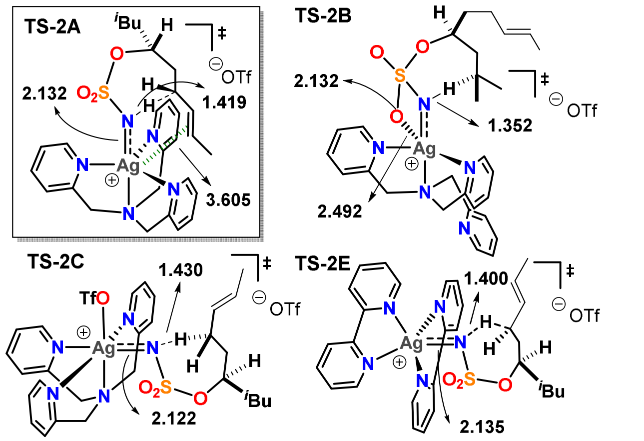

Figure 3. Lowest energy structures of Ag-nitrene transition state complexes (nitrene = NSO_3-(*S*)-CH(^{i}Bu)(Et-(*E*)-CH=CHMe)): **TS-2A-C** and **E**. Distances shown are in Å.

in low-coordinate Ag complexes, and is supported by a crystal structure of Ag-sulfonamide,[35] as well as calculated structures of Ag-nitrene complexes supported by tris(pyrazolyl)borate (Tp) ligands.[36] Ring strain is imposed on the 7-membered TS, disfavoring activation of the allylic C–H bonds. Combining these findings, we conclude that **2B** and **2C** do not agree as well with experiment as does **2A**, suggesting that similar $^-$OTf-free species are also the most important reactive species in benzylic (**1A**) and propargylic (**3A**) C–H amination.

Figure 4 shows the favored *pro-syn* and *pro-anti* **RC-3A** structures for propargylic (**Pg**) vs. **T** C-H bond amination. Calculations show that, despite an experimental *syn:anti* ratio of 3.1:1, only **RC-3A$_{anti}$** contains interactions between Ag and the ethynyl group at 3.89 Å. This interaction is absent in **RC-3A$_{syn}$**, where the rigidity of the ethynyl group rotates it away from Ag when the *pro-syn* **Pg** C-H bond is proximal to the metal. The stabilizing Ag-ethynyl interaction lowers **RC-3A$_{anti}$** by 3.29 kcal·mol^{-1} relative to **RC-3A$_{syn}$**. Stabilization of **RC-3A$_{anti}$** disfavors **TS-3A$_{syn}$** and **TS-3A$_{ter}$** under the Curtin-Hammett-corrected condition, decreasing the preference of **3A** for the *syn* product. This effect is less prominent in **RC-1A** ($\Delta G_{anti} < \Delta G_{syn}$ by 1.31 kcal·mol^{-1}) and **RC-2A** ($\Delta G_{anti} > \Delta G_{syn}$ by 0.23 kcal·mol^{-1}), hence **1A** and **2A** display high *syn dr*. The Ag···π interaction between Ag and the ethynyl π electrons in **3A$_{anti}$** provides an excellent example of NCI-tuned regio- and diastereoselectivity, despite the fact that the interaction reduces *dr* by stabilizing the minor diastereomer.

*Potential energy surfaces for intramolecular NT by **1A**, **2A** and **3A***. To better understand the NT mechanism of [Ag(tpa)]$^+$ and the driving force behind its regio- and stereoselectivities, DFT calculations were performed to study potential energy surfaces (PESs) for regioselective intramolecular NTs between 3° C-H and benzylic C–H (**1A**), allylic C–H (**2A**) and propargylic C–H bonds (**3A**) (Figure 5). In each case, **RC**s and **TS**s corresponding to 3° C–H insertion and the *syn* and *anti* diastereomers resulting from insertion at the α-conjugated C–H bond were considered. For **RC** and **TS** species, the triplet states are uniformly lower in energy; thus, only triplet states are shown in Figure 5. All PESs are similar in three ways: 1) NT proceeds on the triplet surface and spin crossover ensues after the TS (product-determining step, PDS), 2) the NT is initiated via initial H-atom transfer to the nitrene radical anion (both H^+ and e^- are accepted by nitrene$^{\bullet -}$) to yield an organic radical tethered to an Ag(II)tpa-amide species and 3) the NT

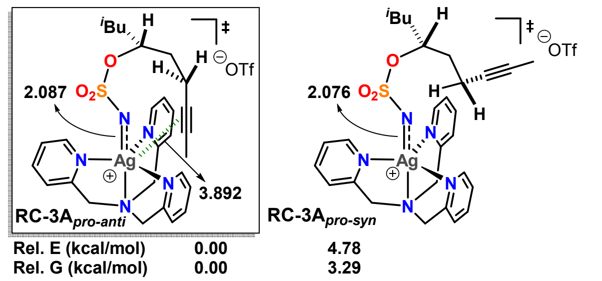

Figure 4. Reactant complex of Ag-nitrene complexes (nitrene = NSO_3-(*S*)-CH(^{i}Bu)(Et-C≡CMe)): **RC-3A$_{pro\text{-}anti}$** and **RC-3A$_{pro\text{-}syn}$**. Distance: Å. Relative single point/Gibbs free energies: kcal·mol^{-1}.

completes on the open-shell singlet (BS(1,1); broken-symmetry formalism) surface via radical recombination (RR) to produce the nitrene-inserted organic product and Ag(I)(tpa). The NT may proceed by: a) an elementary step with barrierless radical recombination occurring immediately after the HT, *E*-HT/RR or b) a fast stepwise recombination, designated as an *S*-HT/RR mechanism. The distinguishing feature of *S*-HT/RR is that diradical intermediates are encountered on both the $^{BS(1,1)}$PES (broken symmetry singlet with two antiferromagnetically coupled unpaired electrons) and ^{3}PES, whereas the *E*-HT/RR mechanism has an intermediate only on the ^{3}PES. NTs occurring via *E*-HT/RR give diastereospecific products, similar to Pérez's[35] [Ag(Tp)]$^+$ and our previously reported [$Ag_2(tpy)_2$OTf]$^+$ systems.[16e] NTs that occur via *S*-HT/RR allow potential scrambling of diastereomers and radical inhibition when the resulting Ag(II)-amide complexes have a triplet ground state.[17e,36]

A look at the PESs for **1A**, **2A** and **3A** shows that, in each case, the energetic ordering of the **RC**s and **TS**s differ (Figure 5, e.g., *anti* < *syn* < 3° are observed for **RC-1A**, while the order is *syn* < *anti* < 3° for **TS-1A**). Thus, product selectivity can be governed solely through kinetic-only control, or by a combination of kinetic and pre-equilibrium control (Curtin-Hammett 'corrected', see Figure S-1). The relative TS energetics were determined under both kinetic-only and Curtin-Hammett regimes. The selectivity pattern is identical for **1A** and **2A**; thus, we cannot distinguish whether the reactions proceed under kinetic-only or Curtin-Hammett-corrected control. For **1A**, the energy ordering of the **TS**s is *syn* < *anti* < 3°, whether calculated from the lowest energy conformer of the **RC**s (SI, eq. 5, Table S-16) or from their respective **RC** conformers (SI, eq. 2). The calculated trend is consistent with experiment, in that only the *syn* product is observed from benzylic C–H insertion and qualitatively consistent with experimental regioselectivity, despite overestimation of benzylic C–H activation. All three reactions proceed through the *E*-HT/RR mechanism to give the organic products after spin-crossover, with *dr* governed by the relative energy between **TS-1A$_{syn}$** and **TS-1A$_{anti}$**, which translates to >20:1 *dr* (*syn*:*anti*), consistent with the experimentally observed *dr*. Similarly, the energy ordering of the **TS**s in the case of **2A** is unaffected by the starting conformer of the **RC**; the trend is *syn* < *anti* < 3°, qualitatively consistent with the observed regioselectivity (**Al**:**T** = experimental 6.6:1 vs. DFT > 19:1) and *dr* (*syn*:*anti* = expt. 13.6:1 vs. DFT 16.2:1) (Figure 5, Table S-19).

The propargylic case represented by **3A** is very different from the benzylic and allylic cases denoted by **1A** and **2A** (Figure 5). Computed selectivities differ depending on whether they are calculated under kinetic-only (SI, eq. 2; Table S-22) or Curtin-Hammett control (SI, eq. 5). The trend is 3° < *syn* < *anti* using Curtin-Hammett control; in contrast, the trend is *syn* < 3° < *anti*

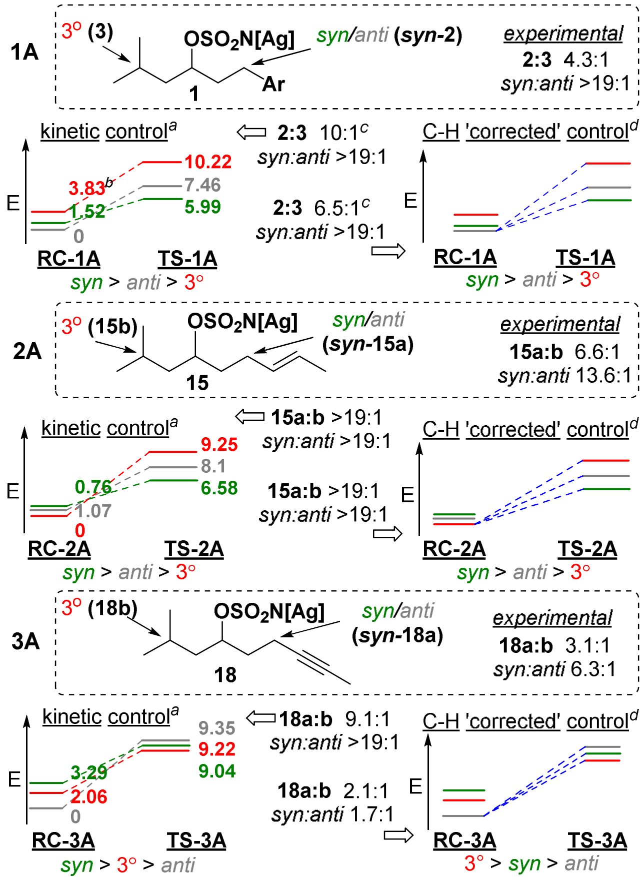

[a] Product distribution calculated using eq. 2 (see SI). [b] Relative energies for Gibbs free energy with dispersion and solvent corrections in kcal mol^{-1}. [c] Selectivities were calculated without the D3 correction. [d] Product distribution calculated using eq. 5 (see SI).

Figure 5. Kinetic-only-controlled and Curtin-Hammett 'corrected' regio- and diastereoselectivities of **1-3A**.

under kinetic control. The dependence of the energy ordering of the **TS** on the **RC** conformation allows us to test the paradigm of the Curtin-Hammett principle as applied to Ag-catalyzed NT. Based on the former orderings of **TS-3A**, the calculated regioselectivity is 3°:propargylic = 1:2.1 (DFT) vs. the 1:3.1 experimental value (using **18a**:**18b** in Table 4 as a model for **3A**) and the calculated *dr* is *syn*:*anti* = 1.7:1 (DFT) vs. a *syn*:*anti* = 6.3:1 experimental ratio. In contrast, kinetic-only control gives calculated regioselectivity for 3°:propargylic of 1:6.5 (DFT) vs. experimental = 1:3.1, while the predicted *syn*:*anti* = >20:1 (DFT) compares to an experimental *syn*:*anti* = 6.3:1. Both models give calculated regioselectivities in reasonable agreement with experiment. However, *dr* is overestimated by the kinetic-only model, because the 7-membered *pro-anti* TS brings the alkynyl group in proximity to the catalyst, resulting in repulsive steric interactions. The unfavorable conformation enforced by the *pro-anti* TS is the reason for high *syn dr* in the case of **1A** and **2A**. On the other hand, *syn dr* for **3A** is mitigated in the Curtin-Hammett-corrected model when the pre-TS equilibrium is considered; the *pro-anti* RC-**3A** posits the alkynyl group next to the Ag center, allowing attractive NCIs to direct NT into the *pro-anti* C–H bond (Figure 4). These results highlight the flexibility of the Ag coordination sphere as a catalyst design principle in these complexes for site-selective NT.

Summarizing the computational results, we suggest that the active Ag-nitrene complexes exist in form **A**, counteranion-free and η^4-tpa (Figures 2-4). The key feature of the Ag complex in form **A**, compared to NT catalysts based on Rh, Ru, and Fe, is a less saturated coordination sphere with an open site located *cis* to the Ag-nitrene bond. This coordination environment, unique to Ag and other Group 11 elements, allows sufficient space between pyridyl rings of the tpa ligand to interact with substrates when NCIs such as π-stacking are applicable, exemplified in **1** and **11-14** and **20–24** (Table 5, *vide infra*). In addition, the fourth coordination site on Ag *cis* to the Ag-nitrene bond allows NCIs between π-electrons in substrates and the metal, as in **15–19** and **20-24**. NCIs are thus important in tuning the energetics among **TS**s and different accessible reactant conformers, impacting the regioselectivity and *dr* of NTs promoted by Ag(tpa)OTf.

Predicting selectivity between competing α-conjugated C–H bonds. In addition to highlighting the potential for NCIs to drive selectivity in Ag-catalyzed NT, we explored if our experimental and computational data might be utilized to predict site-selectivity in new sets of substrates with competing α-conjugated C–H bonds (Table 5). Experimental predictions of product distributions with **20-24** were calculated in the following manner: the selectivities for each of the α-conjugated C–H bonds in **20-24** vs. an isopropyl 3° alkyl C(sp^3)–H bond were gleaned from Tables 1-4. The two

Table 5. Predicted and experimental comparisons of nitrene transfer with substrates containing competing NCIs.

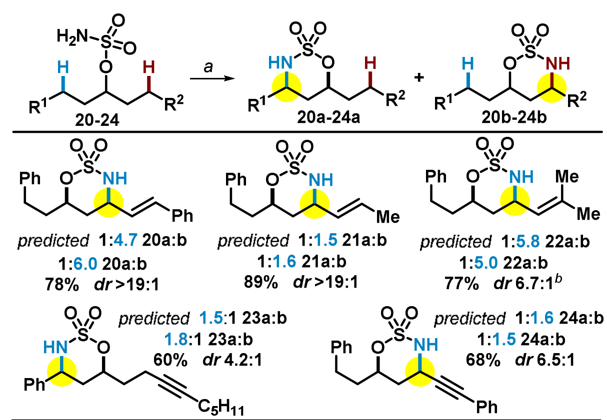

[a] 10 mol % Ag(tpa)OTf, 3.5 equiv PhIO, 0.05 M $CHCl_3$, 4 Å MS, -20 °C. [b] 5% rearranged aziridination product.

numbers were divided to predict which α-conjugated C-H bond in **20-24** is favored. For example, to predict selectivity for **20** with Ag(tpa)OTf at -20 °C in $CHCl_3$, the selectivity for allylic C-H activation in **17** (>19:1, Table 4) is divided by that for benzylic C–H activation in **1** (4.3:1, Table 2) to give ~20/4.3 = 4.7:1. The experimental value for **20a**:**b** is 6.0:1 (Table 3); an accurate match, given that the **17a**:**b** ratio was measured by ^{1}H NMR. Extending this analysis to **21-24** gave predicted ratios for **21-24a**:**21-24b**, close to experimental values. We anticipate that this simple model can be extended to NTs catalyzed by other metals.

This simple predictive model is based on a transition state equivalent to Hess's law (Scheme 4). The underlying assumption is that the potential energy surfaces for the isopropyl reference points are negligibly different (i.e., **1C-RC**$_{ter}$ ≈ **2C-RC**$_{ter}$). For example, the selectivity in **21** and **23** are computationally modeled using the enthalpies and entropies of activation previously calculated for **1A**$_{Bn}$, **2A**$_{Al}$, and **3A**$_{Pg}$ relative to their corresponding

$\mathbf{RC_{ter}}$, similar to tabulated enthalpies and entropies of formation for molecules relative to the most stable form of the constituting elements. In this manner, regioselectivities for **21** and **23** can be estimated without computing entire potential energy surfaces for the nitrene complexes of **21** and **23**, respectively. This method is identical to the simple division procedure employed in Table 5.

Scheme 4. Transition state Hess's law.

$$\begin{array}{llll} & \mathbf{RC_{ter}\text{-}2C} \rightleftharpoons \mathbf{TS_{\mathit{syn}}\text{-}2A} & \Delta G^{\ddagger}(\mathbf{TS_{\mathit{syn}}\text{-}2A}) \\ - & \mathbf{RC_{ter}\text{-}1C} \rightleftharpoons \mathbf{TS_{\mathit{syn}}\text{-}1A} & \Delta G^{\ddagger}(\mathbf{TS_{\mathit{syn}}\text{-}1A}) \\ \hline & \mathbf{TS_{syn}\text{-}1A} \rightleftharpoons \mathbf{TS_{\mathit{syn}}\text{-}2A} & \because \mathbf{RC_{ter}\text{-}1C} = \mathbf{RC_{ter}\text{-}2C} \\ \cong & \mathbf{TS_{Bn}\text{-}21} \rightleftharpoons \mathbf{TS_{Allylic}\text{-}21} & \Delta G\ (\mathbf{21}) \end{array}$$

Table 6. Calculated vs. experimental regioselectivities and *dr* of **21** and **23** under Curtin-Hammett-corrected (CH) control.

Regioisomer (**X**)	calc. **Bn**:**X**[a] (exp.)	calc. *syn:anti* (exp.)
Al (21a:21b)	1:1.26 (1:1.6)	>19:1 (>19:1)
Pg (23a:23b)	1:1.53 (1.8:1)	1.7:1 (4.2:1)

[a]Selectivities were calculated from the relative energy of $\mathbf{TS\text{-}1A_{Bn}}$ with respect to (w.r.t.) $\mathbf{RC\text{-}1C_{ter}}$ and $\mathbf{TS\text{-}2A_{Al}}$ w.r.t. $\mathbf{RC\text{-}2C_{ter}}$ for **21** and the relative energy of $\mathbf{TS\text{-}1A_{Bn}}$ w.r.t. $\mathbf{RC\text{-}1C_{ter}}$ and $\mathbf{TS\text{-}3A_{Al}}$ w.r.t. $\mathbf{RC\text{-}3C_{ter}}$ for **23**.

"Attractive" vs repulsive NCIs in ligand-tunable Ag-catalyzed regioselective NT. "Attractive" NCIs (namely, Ag···π and π···π interactions) are a complementary strategy to steric-driven, repulsive NCIs for tuning regioselectivity in metal-catalyzed NT. Both types of NCIs enable catalyst control over the NT, rather than substrate control dictated by differences in the BDEs of the targeted C–H bonds, for example. We have also demonstrated that while **2A** and **2E** share identical metal centers and similar donor ligands (Figure 3 for computations), the two catalysts display opposite regioselectivities in most cases.[17a]

To further demonstrate the importance of attractive vs. repulsive NCIs in impacting selectivity of NT, **1A** and [Ag(tpa)(NSO_3-(*R*)-(^{i}Bu)(CH_2Cy))]$^+$ (**4A**, Cy = cyclohexyl) (Figure 6) were compared experimentally and computationally. The three functional groups containing the abstracted γC–H bonds (^{i}Pr and Bn in **1**, and ^{i}Pr and Cy in **4A**), form a sterically similar triad to minimize interference from repulsive NCIs in our analysis. Steric values as measured by Tolman's cone angles are ^{i}Pr, 160; Bn, 165; and Cy, 170;[37] Charton values are 0.76, 0.7, and 0.87 and Sterimol values 1.9, 1.9 and 1.9, respectively.[38] Despite having similar steric profiles, experimentally observed ratios of ^{i}Pr:Bn and ^{i}Pr:Cy are highly catalyst-dependent (1:2.8 and 1.4:1 for Ag(tpa)OTf, compared to inverted trends of 2.8:1 and 1:3.5 with $Ag(tBu_2bpy)_2OTf$, not shown).[17a,39] This highlights the fact that Ag-catalyzed NT in these cases is not operating under substrate-controlled regioselectivity. Computationally, we predict an ^{i}Pr:Bn ratio of 8.1:1 for **4A** (with CH correction and without D3 correction for consistency with calculations on **1A**), which is slightly overestimated from the experimentally observed ratio of 1.4:1. **4A** contrasts with **1A** in terms of regioselectivity, despite the similar steric features of Bn and Cy. This mirrors the respective Ag–N and N···γH distances during the TS; breakage of the Ag–N bond occurs before formation of the N···γH bond begins in $\mathbf{TS\text{-}4A_{ter}}$, as compared to $\mathbf{TS\text{-}4A_{Cy}}$, implying that approach of the Cy group is hindered in the TS. Elongation of the Ag–N bond, which increases the activation energy, is required to lessen the repulsive NCIs to access $\mathbf{TS\text{-}4A_{Cy}}$. A different scenario is seen in **1A**, where $\mathbf{TS\text{-}1A_{Bn}}$ contains the longest N···γH bond, despite displaying the shortest Ag–N bond among the three TS structures in Figure 6. These bond features signal a very early transition state for $\mathbf{TS\text{-}1A_{Bn}}$ and rule out substrate-controlled regioselectivity for benzylic C–H abstraction (a more exothermic HAT and electron transfer are ruled out from the long N···γH bond and short Ag–N bond, respectively). This early TS is a result of preorganization of the TS structure due to attractive NCIs, further support that the Ag(tpa)$^+$ catalyst operates via an overall attractive NCIs for **1A** vs. repulsive NCIs for **4A**.

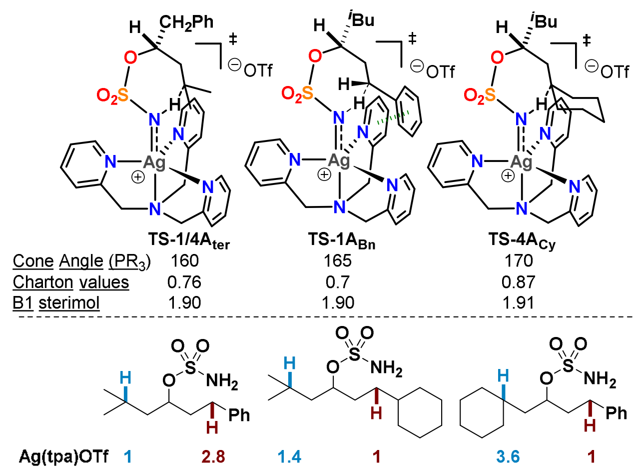

Figure 6. Ag-nitrene transition state complexes: $\mathbf{TS\text{-}1/4A_{ter}}$, $\mathbf{TS\text{-}1A_{Bn}}$ and $\mathbf{TS\text{-}4A_{ter}}$. Distances are in Å. Steric parameters are shown for proximal groups containing the abstracted C–H bond.

Conclusions.

Intramolecular NT reactions catalyzed by Ag(tpa)OTf were found to be influenced by weak NCIs between the substrate and the catalyst. Experimentally, competitive amination was probed in a number of bifunctional substrates, including benzylic vs. 3°, allylic vs. 3°, propargylic vs. 3°, benzylic vs. allylic, and benzylic vs. propargylic C–H bonds. Excellent yields and site-selectivities are observed in a number of cases, where contributions from NCIs are strongly implicated in determining the selectivity. These non-covalent interactions were probed computationally in detail. Both substrate aryl···tpa-pyridyl π···π interactions and Ag···π interactions were clearly observed in the lowest-energy Ag-nitrene structures and transition states. We further showed how the experimentally determined selectivities and calculated transition states can be used to predict selectivities for new substrates that contain competing NCIs. These results set the stage for future catalyst developments that integrate non-covalent directing effects as a design element for group transfer reactions. This strategy complements previous reliance on inherent steric and electronic features of reactive metal-nitrene intermediates to dictate selectivity.

ASSOCIATED CONTENT

Supporting Information

Experimental procedures and characterization data for all new compounds are available in the Supporting Information. This material is available free of charge at http://pubs.acs.org.

AUTHOR INFORMATION

Corresponding Authors

berry@chem.wisc.edu
schomakerj@chem.wisc.edu

ǂ These authors contributed equally.

Notes

The authors declare no competing financial interests.

ACKNOWLEDGMENT

This work was funded through the Wisconsin Alumni Research Foundation (WARF) and NSF-1664374 to JMS. The NMR facilities at UW-Madison are funded by NSF (CHE-1048642, CHE-0342998) and NIH S10 OD012245. The NMR Facility at Madison is supported by NIH (P41GM103399, S10RR08438, S10RR029220) and NSF (BIR-0214394). JFB thanks the Center for Selective C–H Functionalization supported by the NSF (CHE01205646). The computational facility at Madison is supported in part by NSF Grant CHE-0840494 and at the UW-Madison Center for High Throughput Computing (CHTC) in the Department of Computer Sciences. The CHTC is supported by UW-Madison, the Advanced Computing Initiative, the WARF, the Wisconsin Institutes for Discovery, and the NSF, and is an active member of the Open Science Grid, which is supported by NSF and the U.S. DOE Office of Science. U.S. Chimera is developed by the Resource for Biocomputing, Visualization, and Informatics at UCSF (supported by NIGMS P41-GM103311).

REFERENCES

1. For selected references on directed C-H functionalization, see: a) Rouquet, G.; Chatani, N. *Angew. Chem. Int. Ed.* **2013**, *52*, 11726. b) Wang, C.; Huang, Y. *Synlett* **2013**, *24*, 145. c) Rousseau, G.; Breit, B. *Angew. Chem. Int. Ed.* **2011**, *50*, 2450. d) Song, G.; Wang, F.; Li, X. *Chem. Soc. Rev.* **2012**, *41*, 3651. e) Yu, J-.Q.; Giri, R.; Chen, X. *Org. Biomol. Chem.* **2006**, *4*, 4041. f) Patureau, F.W.; Glorious, F. *Angew. Chem. Int. Ed.* **2011**, *50*, 1977. g) Engle, K M.; Mei, T-.S.; Wasa, M.; Yu, J-.Q. *Acc. Chem. Res.* **2011**, *45*, 788. h) Colby, D.A.; Tsai, A.S.; Bergman, R.G.; Ellman, J.A. *Acc. Chem. Res.* **2011**, 814. i) Shul'pin, G. B. *Org. Biomol. Chem.* **2010**, *8*, 4217.

2. For selected references on non-directed C-H functionalization, see: a) Das, S.; Incarvito, C.D.; Crabtree, R.H.; Brudvig, G.W. *Science* **2006**, *312*, 1941. b) Crabtree, R.H. *J. Chem. Soc. Dalton Trans.* **2001**, 17, 2437. c) Hashiguchi, B.G.; Bischof, S.M.; Konnick, M.M.; Periana, R.A. *Acc. Chem. Res.* **2012**, *45*, 885. d) Balcells, D.; Eisenstein, O. *Chem. Rev.* **2010**, *110*, 749. e) Kuhl, N.; Hopkinson, M.M.; Wencel-Delord, J.; Glorius, F. *Angew. Chem. Int. Ed.* **2012**, *51*, 10236. f) Arndtsen, B.A.; Bergman, R.G.; Mobley, T.A.; Peterson, T.H. *Acc. Chem. Res.* **1995**, *28*, 154. g) Wencel-Delord, J.; Glorius, F. *Nat. Chem*. **2013**, *5*, 369. h) Wencel-Delord, J.; Dröge, T.; Liu, F.; Glorius, F. *Chem. Soc. Rev.* **2011**, *40*, 4740. i) Shul'pin, G.B. *Dalton Trans.* **2013**, *42*, 12794

3. References on synthesis and importance of amines, see: a) Lawrence, S.A. *Amines: Synthesis, Properties and Applications* (Cambridge University Press, New York, NY, **2004**. b) Nugent, T.C.; El-Shazly, M. *Adv. Synth. Cat.* **2010**, *352*, 753. c) Smith, M.B. in *Compendium of Organic Synthetic Methods* Wiley, New York, NY, vol. 12, **2009**. d) Emerson, W.S. *The Preparation of Amines by Reductive Alkylation* in *Organic Reactions* Wiley, New York, NY, **2004**. e) Afagh, N.A.; Yudin, A.K. *Angew. Chem. Int. Ed.* **2010**, *49*, 262.

4. Reviews on nitrene transfer: a) Zalatan, D.N.; Du Bois, J. *Top. Curr. Chem.* **2010**, *292*, 347. b) Muller, P.; Fruit, C. *Chem. Rev.* **2003**, *103*, 2905. c) Li, Z.G.; He, C. *Eur. J. Org. Chem.* **2006**, *19*, 4313. d) Halfen, J. A. *Curr. Org. Chem.* **2005**, *9*, 657. e) Dequirez, G.; Pons, V.; Dauban, P. *Angew. Chem. Int. Ed.* **2012**, *51*, 7384. f) Collet, F.; Dodd, R.H.; Dauban, P. *Chem. Commun.* **2009**, *34*, 5061. g) Collet, F.; Lescot, C.; Dauban, P. *Chem. Soc. Rev.* **2011**, *40*, 1926. h) Degennaro, L.; Trinchera, P.; Luisi, R. *Chem. Rev.* **2014**, *114*, 7881.

5. Selected reviews of Rh-catalyzed nitrene transfer: a) Roizen, J.L.; Harvey, M.E.; Du Bois, J. *Accts. Chem. Res.* **2012**, *45*, 911. b) Collet, F.; Lescot, C.; Liang, C.G.; Dauban, P. *Dalton Trans.* **2010**, *39*, 10401. For Ag, see: c) Gómez-Emeterio, B.P.; Urbano, J.; Díaz-Requejo, M.M.; Pérez, P.J. *Organometallics* **2008**, *27*, 4126. d) Kornecki, K. P.; Powers, D. C.; Ritter, T.; Berry, J. F. *Prog. Inorg. Chem.* **2014**, *58*, 225. e) Kornecki, K. P.; Berry, J. F. *Chem. Eur. J.* **2011**, *17*, 5827.

6. For selected early examples of Ag-catalyzed nitrene transfer, see: a) Cui, Y.; He, C. *J. Am. Chem. Soc.* **2003**, *125*, 16202. b) Cui, Y.; He, C. *Angew. Chem. Int. Ed.* **2004**, *43*, 4210. c) Li, Z.; Capretto, D.A.; Rahaman, R.H.; He, C. *Angew. Chem. Int. Ed.* **2007**, *46*, 5184. d) Llaveria, J.; Beltran, A.; Diaz-Requejo, M.M.; Matheu, M.I.; Castillon, S.; Perez, P.J. *Angew. Chem. Int. Ed.* **2010**, *49*, 7092.

7. Co/Pd-catalyzed nitrene transfer, see: Huang, G. –H.; Li, J.-M.; Huang, J.-J.; Lin,; J.-D.; Chuang, G. J. *Chem. Eur. J.* **2014**, *20*, 5240.

8. Selected examples of Ru-catalyzed nitrene transfer: a) Au, S.-M.; Fung, W.–H.; Cheng, M.-C.; Che, C.-M.; Peng, S.-M. *Chem. Commun.* **1997**, 1655. b) Au, S.-M.; Huang, J.-S.; Che, C.-M.; Yu, W.-Y. *J. Org. Chem.* **2000**, *65*, 7858. c) Harvey, M.E.; Musaev, D.G.; Du Bois, J. *J. Am. Chem. Soc.* **2011**, *133*, 17207. d) Takaoka, A.; Moret, M.-E.; Peters, J. C. *J. Am. Chem. Soc.* **2012**, *134*, 6695. e) Takaoka, A.; Gerber, L. C. H.; Peters, J. C. *Angew. Chem. Int. Ed.* **2010**, *49*, 4088. f) Fantauzzi, S.; Gallo, E.; Caselli, A.; Ragaini, F.; Casati, N.; Macchic, P.; Cenini, S. *Chem. Commun.* **2009**, 3952.

9. For selected examples of Cu-catalyzed nitrene transfer, see: a) Evans, D. A.; Faul, M.M.; Bilodeau, M.T. *J. Org. Chem.* **1991**, *56*, 6744. b) Evans, D. A.; Faul, M.M. Bilodeau, M.T. *J. Am. Chem. Soc.* **1994**, *116*, 2742. c) Dielmann, F.; Andrada, D. M.; Frenking, G.; Bertrand, G. *J. Am. Chem. Soc.* **2014**, *136*, 3800.

10. Selected references on Co-catalyzed nitrene transfer: a) Lu, H.J.; Subbarayan, V.; Tao, J.R.; Zhang, X.P. *Organometallics* **2010**, *29*, 389-393. b) Lu, H.-J.; Jiang, H.-L.; Hu, Y.; Wojtas,L.; Zhang, X.P. *Org. Lett.* **2012**, *14*, 5158–5161. c) Lu, H.-J.; Jiang, H.-L.; Hu, Y.; Wojtas, L.; Zhang, X.P. *Chem. Sci.* **2011**, *2*, 2361–2366. d) Lu, H.-J.; Jiang, H.-L.; Wojtas, L.; Zhang, X.P. *Angew. Chem. Int. Ed.* **2010**, *49*, 10192–10196. e) Lu, H.-J.; Li, C.-Q.; Jiang, H.-L.; Lizardi, C.L.; Zhang, X.P. *Angew. Chem. Int. Ed.* **2014**, *53*, 7028–7032.

11. For examples with Fe, see: a) Kuppuswamy, S.; Powers, T. M.; Johnson, B. M.; Bezpalko, M. W.; Brozek, C. K.; Foxman, B. M.; Berben, L. A.; Thomas, C. M. *Inorg. Chem.* **2013**, *52*, 4802. b) King, E. R.; Hennesy, E. T.; Betley, T. A. *J. Am. Chem. Soc.* **2011**, *133*, 4917. c) Bowman, A. C.; Milsmann, C.; Bill, E.; Turner, Z. R.; Lobkovsky, E.; DeBeer, S.; Wieghardt, K.; Chirik, P. J. *J. Am. Chem. Soc.* **2011**, *133*, 17353.

12. a) Hayes, C.J.; Beavis, P.W.; Humphries, L.A. *Chem. Commun.* **2006**, 4501. b) Fiori, K.W.; Du Bois, J. *J. Am. Chem. Soc.* **2007**, *129*, 562. c) Zalatan, D.N.; Du Bois, J. *J. Am. Chem. Soc.* **2008**, *130*, 9220. d) Kornecki, K.P.; Berry, J.F. *Eur. J. Inorg. Chem.* **2012**, *3*, 562. e) Cramer, S.A.; Jenkins, D. M. *J. Am. Chem. Soc.* **2011**, *133*, 19342. f) Hennessy, E. T.; Liu, R.Y.; Iovan, D.A.; Duncan, R. A.; Betley, T. A. *J. Am. Chem. Soc.* **2014**, *5*, 1526. g) Srivastava, R.S.; Tarver, N.R.; Nicholas, K.M. *J. Am. Chem. Soc.* **2007**, *129*, 15250. h) Barman, D.N.; Nicholas, K.M. *Eur. J. Org. Chem.* **2011**, *5*, 908. i) Davies, H.M.L.; Manning, J.R. *Nature* **2008**, *451*, 417. j) Ramirez, T.A.; Zhao, B.; Shi, Y. *Chem. Soc. Rev.* **2012**, *41*, 931.

13. Fiori, K.W.; Espino, C.G.; Brodsky, B.H.; Du Bois, J. *Tetrahedron* **2009**, *65*, 3042.

14. Selected references, see: a) Milo, A.; Neel, A.J.; Toste, F.D.; Sigman, M.S. *Science* **2015**, *347*, 737. b) Krenske, E.H.; Houk, K.N. *Acc. Chem. Res.* **2013**, *46*, 979. c) Knowles, R.R.; Jacobsen, E.N. *Proc.*

Natl. Acad. Sci. U.S.A. **2010**, *107*, 20678. d) Wheeler, S.E.; Bloom, J.W.G. *J. Phys. Chem. A* **2014**, *118*, 6133. e) Houk, K.N.; Cheong, P. H.-Y. *Nature* **2008**, *455*, 309. f) Neel, A.J.; Hilton, M.J.; Sigman, M.S.; Toste, F.D. *Nature* **2017**, *543*, 637. g) Evans, D.A.; Faul, M.M.; Bilodeau, M.T. *J. Am. Chem. Soc.* **1994**, *116*, 2742. h) Li, Z.; Conser, K.R.; Jacobsen, E.N. *J. Am. Chem. Soc.* **1993**, *115*, 5326.

15. Suarez, A.I.O.; Jiang, H.; Zhang, X.P.; de Bruin, B. *Dalton Trans.* **2011**, *40*, 5697-5705 and references therein.

16. a) Hung-Low, F.; Renz, A.; Klausmeyer, K.K. *Polyhedron* **2009**, *28*, 407. b) Hung-Low, F.; Renz, A.; Klausmeyer, K.K. *J. Chem. Cryst.* **2011**, *41*, 1174. c) Du, J.; Hu, T.; Zhang, S.; Zeng, Y.; Bu, X. *CrystEngComm.* **2008**, *10*, 1866. d) Zhang, H.; Chen, L.; Song, H.; Zi, G. *Inorg. Chim. Acta* **2011**, *366*, 320. e) Hung-Low, F.; Renz, A.; Klausmeyer, K.K. *J. Chem. Cryst.* **2009**, *39*, 438. f) Levason, W.; Spicer, M.D. *Coord. Chem. Rev.* **1987**, *76*, 45. g) Leschke, M.; Rheinwald, G.; Lang, H. *Z. Anorg. Allg. Chem.* **2002**, *628*, 2470. h) Zhu, H.-L.; Chen, Q.; Peng, W.-l.; Qi, S.-J.; Xu, S.-J.;Xu, A.-L.; Chen, X.-M. *Chin. J. Chem.* **2001**, *19*, 263. i) Bowmaker, G. A.; Effendy; Marfuah, S.; Skelton, B. W.; White, A. H. *Inorg. Chim. Acta* **2005**, *358*, 4371. j) Paramonov, S. E.; Kozmina, N. P.; Troganov, S. I. *Polyhedron* **2003**, *22* 837. k)Han, Z.; Wang, Y.; Wu, J.; Zhai, X. *Solid State Sci.* **2011**, *13*, 1560. l) Yuan, L.; Qin, C.; Wang, X.; Li, Y.; Wang, E. *Dalton Trans.* **2009**, 4169.

17. a) Alderson, J. A.; Phelps, A. M.; Scamp, R. J.; Dolan, N. S.; Schomaker, J. M. *J. Am. Chem. Soc.* **2014**, *136*, 16720. b) Rigoli, J. W.; Weatherly, C. D.; Alderson, J. M.; Vo, B. T.; Schomaker, J. M. *J. Am. Chem. Soc.* **2013**, *135*, 17238. c) Rigoli, J.W.; Weatherly, C.D.; Vo, V.T.; Neale, S.; Meis, A.R.; Schomaker, J.M. *Org. Lett.* **2013**, *15*, 290. d) Scamp, R.J.; Rigoli, J.W.; Schomaker, J.M. *Pure Appl. Chem.* **2014**, *86*, 381. e) Dolan, N. S.; Scamp, R. J.; Yang, T.; Berry, J. F.; Schomaker, J. M. *J. Am. Chem. Soc.* **2016**, *138*, 14658-14667. f) Ju, M.; Weatherly, C.D.; Guzei, I.A.; Schomaker, J.M. *Angew. Chem. Int. Ed.* **2017**, *56*, 9944-9948. g) Huang, M.; Corbin, J.R.; Dolan, N.S.; Fry, C.G.; Vinokur, A.; Guzei, I.A.; Schomaker, J.M. *Inorg. Chem.* **2017**, *56*, 6725–6733. h) Alderson, J.M.; Schomaker, J.M. *Chem. Eur. J.* **2017**, *23*, 8571-8576. i) Weatherly, C.D.; Alderson, J.M.; Hein, J.; Berry, J.F.; Schomaker, J.M. *Organometallics* **2017**, *36*, 1649–1661. j) Scamp, R.J.; Jirak, J.G.; Dolan, N.; Guzei, I.; Schomaker, J.M. *Org Lett.* **2016**, *18*, 3014.

18. a) Kristyan, S.; Pulay, P. *Chem. Phys. Lett.* **1994**, *229*, 175. b) Hobza, P.; Sponer, J.; Reschel, T. *Comp. Chem.* **1995**, *16*, 1315. c) Perezjorda, J.M.; Becke, A.D. *Chem. Phys. Lett.* **1995**, *233*, 134. d) Grimme, S.; Antony, J.; Schwabe, T.; Mück-Lichtenfeld, C. *Org. Biomol. Chem.* **2007**, *5*, 741.

19. Bruice, T.C.; Lightstone, F.C. *Acc. Chem. Res.* **1999**, *32*, 127.

20. a) Paradine, S.M.; White, M.C. *J. Am. Chem. Soc.* **2012**, *134*, 2036. b) Paradine, S.M.; Griffin, J.R.; Zhao, J.; Petronico, A.L.; Miller, S.M.; White, M.C. *Nature* **2015**, *7*, 987.

21. a) Zhang, X.; Xu, H.; Zhao, C. *J. Org. Chem.* **2014**, *79*, 9799. b) Varela-Álvarez, A.; Yang, T.; Jennings, H.; Kornecki, K.P.; Macmillan, S.N.; Lancaster, K.M.; Mack, J.B.C.; Du Bois, J.; Berry, J.F.; Musaev, D.G. *J. Am. Chem. Soc.* **2016**, *138*, 2327.

22. Hansch, C.; Leo, A.; Taft, R.W. *Chem. Rev.* **1991**, *91*, 165.

23. a) Kuijpers, P.F.; Tiekink, M.J.; Breukelaar, W.B.; Broere, D.L.J.; van Leest, N.P.; van der Vlugt, J.I.; Reek, J.N.H.; de Bruin, B. *Chem. Eur. J.* **2017**, *23*, 7945-7952. b) Lyaskovskyy, V.; Suarez, A.I.O.; Lu, H.; Jiang, H.; Zhang, X.P.; de Bruin, B. *J. Am. Chem. Soc.* **2011**, *133*, 12264-12273. c) Goswami, M.; Lyaskovskyy, V.; Domingos, S.R.; Buma, W.J.; Woutersen, S.; Troeppner, O.; Ivanovic-Burmazovic, I.; Lu, H.; Cui, X.; Zhang, X.P.; Reijerse, E.J.; DeBeer, S.; van Schooneveld, M.M.; Pfaff, F.F.; Ray, K.; de Bruin, B. *J. Am. Chem. Soc.* **2015**, *137*, 5468-5479.

24. For selected references, see: a) Sinnokrot, M.O.; Valeev, E.F.; Sherrill, C.D. *J. Am. Chem. Soc.* **2002**, *124*, 10887–10893. b) Hunter, C.A.; Sanders, J.K. *J. Am. Chem. Soc.* **1990**, *112*, 5525–5534. c) Cozzi, F.; Cinquini, M.; Annuziata, R.; Siegel, J.S. *J. Am. Chem. Soc.* **1993**, *115*, 5330–5331. d) Burley, S.K.; Petsko, G.A. *Science* **1985**, *229*, 23. e) Shepodd, T.J.; Petti, M.A.; Dougherty, D.A. *J. Am. Chem. Soc.* **1988**, *110*, 1983. f) Sunner, J.; Nishizawa, K.; Kebarle, P. *J. Phys. Chem.* **1981**, 85, 1814. g) Kearney, P.C.; Mizoue, L.S.; Kumpf, R.A.; Forman, J.E.; McCurdy, A.; Doughtery, D.A. *J. Am. Chem. Soc.* **1993**, *115*, 9907. h) Kumpf, R.A.; Dougherty, D.A. *Science* **1993**, *261*, 1708. i) Dougherty, D. *Science* **1996**, *271*, 163.

25. For selected references, see: a) Martinez, C.R.; Iverson, B.L. *Chem. Sci.* **2012**, *3*, 2191. b) Wheeler, S.E.; Houk, K.N. *Mol. Phys.* **2009**, *107*, 749. c) Wheeler, S.E.; Houk, K.N. *J. Am. Chem. Soc.* **2009**, *131*, 3126. d) Wheeler, S.E.; Houk, K.N. *J. Chem. Theory Comput.* **2009**, *5*, 2301. e) Raju, R.K.; Bloom, J.W.G.; An, Y.; Wheeler, S.E. *ChemPhysChem* **2011**, *12*, 3116. f) Bloom, J.W.G.; Wheeler, S.E. *Angew. Chem. Int. Ed.* **2011**, 50, 7847. g) Wheeler, S.E. *J. Am. Chem. Soc.* **2011**, *133*, 10262. h) Wheeler, S.E. *Acc. Chem. Res.* **2013**, *46*, 1029.

26. Janiak, C. *Dalton Trans.* **2000**, 3885.

27. Selected references: a) Dewar, M.J.S. *Bull. Soc. Chim. Fr.* **1951**, *18*, C79. b) Winstein, S.; Lucas, H.J. *J. Am. Chem. Soc*. **1938**, *60*, 836. c) Williams, C.M.; Mander, L.N. *Tetrahedron* **2001**, *57*, 425. d) Cottam, J.R.A.; Steel, P.J. *J. Organometallic Chem.* **2006**, *691*, 2286.

28. a) Breault, G. A.; Hunter, C. A.; Mayers, P. *C. J. Am. Chem. Soc.*, **1998**, *120*, 3402. b) Cubberley, M. S.; Iverson, B. L. *J. Am. Chem. Soc.* **2001,** *123,* 7560. c) Gutmann, V. *Coord. Chem. Rev.* **1976**, *18*, 225. d) Hunter, C. A.; Lawson, K. R.; Perkins, J.; Urch, C. J. *J. Chem. Soc., Perkin Trans. 2*, **2001**, 651.

29. Reichardt, C.; Welton, T. *Solvents and Solvent Effects in Organic Chemistry, 4th Edition*. Wiley-VCH: Verlag GmbH & Co. KGaA, **2011**.

30. Hunter, C.; Sanders, J. K. *J. Am. Chem. Soc.* **1990**, *112*, 5525.

31. For selected references, see: a) Cockroft, S. L.; Hunter, C. A.; Lawson, K. R.; Perkins, Julie; Urch C. J. *J. Am. Chem. Soc.* **2005**, *127*, 8594. b) Cozzi, F.; Ponzini, F.; Annunziata, R.; Cinquini, M.; Siegel, J. S. *Angew. Chem., Int. Ed. Engl.* **1995**, *34*, 1019. c) Newcomb, L. F.; Gellman, S. H. *J. Am. Chem. Soc.* **1994**, *116*, 4993-4994. d) Rashkin, M. J.; Waters, M. L. *J. Am. Chem. Soc.* **2002**, *124*, 1860-1861. e) Cubberley, M. S.; Iverson, B. L. *J. Am. Chem. Soc*. **2001**, *123*, 7560-7563. f) Lai, J. S.; Qu, J.; Kool, E. T. *Angew. Chem., Int. Ed.* **2003**, *42*, 5973-5977. g) Zahn, A.; Brotschi, C.; Leumann, C. J. *Chem.sEur. J.* **2005**, *11*, 2125-2129. h) Hunter, C. A. *Angew. Chem., Int. Ed.* **2004**, *43*, 5310-5324.

32. Maier, J.M.; Li, P.; Hwang, J.; Smith, M.D.; Shimizu, K.D. *J. Am. Chem. Soc.* **2015**, *137*, 8014.

33. Grimme, S.; Hansen, A.; Brandenburg, J.G.; Bannwarth, C. *Chem. Rev.* **2016**, *116*, 5105.

34. a) Bruno, J.; Cole, J.C.; Edgington, P.R.; Kessler, M.; Macrae, C.F.; McCabe, P.; Pearson, J.; Taylor, R. *Acta Cryst.* **2002**, *B58*, 389. b) Cambridge Structural Database, accessed Feb. 22, 2017.

35. Zanvettor, N.T.; Abbehausen, J.; Lustri, W.R.; Cuin, A.; Masciocchi, N.; Corbi, P.P. *J. Mol. Structure* **2015**, *1082*, 180.

36. Maestre, L.; Sameera, W.M.; Díaz-Requejo, M.M.; Maseras, F.; Pérez, P.J. *J. Am. Chem. Soc.* **2013**, *135*, 1338.

37. Tolman, C.A. *Chem. Rev.* **1977**, *77*, 313-348.

38. a) Charton, M. *J. Am. Chem. Soc.* **1975**, *97*, 1552-1556. b) Charton, M. *J. Am. Chem. Soc.* **1975**, *97*, 3691-3693. c) Charton, M. *J. Org. Chem.* **1976**, *41*, 2217-2220. d) Drug Design Ariens, E.J., ed.; Academic Press **1976**, 133. e) Biological Activity and Chemical Structure Buisman, J.A.; ed.; Elsevier **1977**, 63. f) QSAR in Drug Dosing and Toxicology Hadzi. B.; Jerman-Blazic, B.; ed.; Elsevier **1987**, 97. g) IUPAC Pesticide Chemistry Vol. 1 Miyamoto, J.; ed.; Pergamon **1983**, 339.

39. Corbin, J.R.; Schomaker, J.M. *Chem. Commun.* **2017**, *53*, 4346-4349.

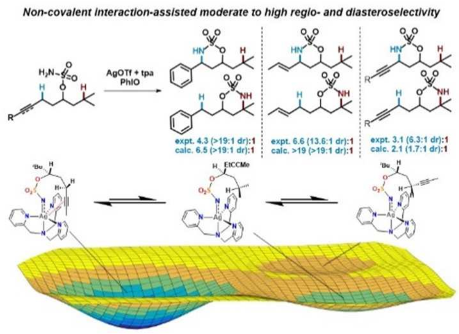
Non-covalent interaction-assisted moderate to high regio- and diasteroselectivity
AgOTf + tpa
PhIO
expt. 4.3 (>19:1 dr):1
calc. 6.5 (>19:1 dr):1
expt. 6.6 (13.6:1 dr):1
calc. >19 (>19:1 dr):1
expt. 3.1 (6.3:1 dr):1
calc. 2.1 (1.7:1 dr):1
EtCCMe